

Article

Estimation of Soil Erosion in the Chaohu Lake Basin through Modified Soil Erodibility Combined with Gravel Content in the RUSLE Model

Sai Hu ^{1,2}, Long Li ^{1,2,3} , Longqian Chen ^{1,2,*}, Liang Cheng ^{1,2,4}, Lina Yuan ^{1,2}, Xiaodong Huang ⁵ and Ting Zhang ^{1,2}

¹ School of Environmental Science and Spatial Informatics, China University of Mining and Technology, Daxue Road 1, Xuzhou 221116, China

² Engineering Research Center of Ministry of Education for Mine Ecological Restoration, China University of Mining and Technology, Daxue Road 1, Xuzhou 221116, China

³ Department of Geography, Earth System Science, Vrije Universiteit Brussel, Pleinlaan 2, 1050 Brussels, Belgium

⁴ College of Yingdong Agricultural Science and Engineering, Shaoguan University, Daxue Road 26, Shaoguan 512005, China

⁵ School of Surveying and Landing Information Engineering, Henan Polytechnic University, Century Road 2001, Jiaozuo 454000, China

* Correspondence: chenlq@cumt.edu.cn; Tel.: +86-516-8359-1327

Received: 8 July 2019; Accepted: 26 August 2019; Published: 29 August 2019



Abstract: It is generally acknowledged that soil erosion has become one of the greatest global threats to the human–environment system. Although the Revised Universal Soil Loss Equation (RUSLE) has been widely used for soil erosion estimation, the algorithm for calculating soil erodibility factor (K) in this equation remains limited, particularly in the context of China, which features highly diverse soil types. In order to address the problem, a modified algorithm describing the piecewise function of gravel content and relative soil erosion was used for the first time to modify the soil erodibility factor, because it has been proven that gravel content has an important effect on soil erosion. The Chaohu Lake Basin (CLB) in East China was used as an example to assess whether our proposal can improve the accuracy of soil erodibility calculation and soil erosion estimation compared with measured data. Results show that (1) taking gravel content into account helps to improve the calculation of soil erodibility and soil erosion estimation due to its protection to topsoil; (2) the overall soil erosion in the CLB was low ($1.78 \text{ Mg}\cdot\text{ha}^{-1}\cdot\text{year}^{-1}$) the majority of which was slight erosion (accounting for 85.6%) and no extremely severe erosion; and (3) inappropriate land use such as steep slope reclamation and excessive vegetation destruction are the main reasons for soil erosion of the CLB. Our study will contribute to decision-makers to develop soil and water conservation policies.

Keywords: soil erosion; RUSLE; soil erodibility; gravel content; Chaohu Lake Basin

1. Introduction

Soil erosion has become a major global environmental hazard [1], posing a serious threat to the ecological environment, natural resources, and socio–economic development [2,3]. It often has a negative impact on downstream areas, including lowered water levels in reservoirs [4], threats from floods and mudslides [5], damage to habitats of species [6], and reduced agricultural productivity [7,8]. For example, the Mediterranean vineyards are among the most degraded agricultural ecosystems affected by extreme soil erosion rates [9,10], and this situation has also been observed in citrus plantations [11,12]. As one of the most severe areas of soil erosion in the world, the Loess Plateau in

China has caused great damage to the natural environment, and the economic and social development of the region [13]. It is acknowledged that soil erosion has become a major threat to sustainability due to the immediate damage it causes to the soil system and the acceleration of the land degradation process [12]. Soil erosion is a natural process that is controlled by a variety of environmental factors, such as topography, soil, climate, and vegetation [14]. Human activities, for example, deforestation, agricultural production, and construction, accelerate the rate of soil erosion [2,15]. The United Nations (UN) has highlighted soil and water protection as a key land-use policy issue, which is an effective manner to address the challenges of the UN Sustainable Development Goals [16,17]. In general, estimation of soil erosion provides a basis for soil and water conservation [18].

Quantitative modeling, either physically based or empirically based, has become a widely accepted approach in soil erosion estimation research [19,20]. At present, many empirical models have been developed for estimating soil erosion [1]. Among them, the Revised Universal Soil Loss Equation (RUSLE) has become the most commonly used in different environmental conditions and on varying scales [21–25]. The parameter factors in the RUSLE model include rainfall erosivity, soil erodibility, slope length and steepness, cover fraction, and support practice [26], as soil erosion is the result of a combination of natural and human factors [27].

Topography is one of the factors determining the amount of soil erosion, and slope plays an important role in increasing soil loss [28]. Smith and Wischmeier first found that soil loss was a polynomial function of slope (θ) [29] and later modified this function by creating the slope factor, which is a polynomial function of the sine of slope ($\sin \theta$; see Equation (9)) as it could improve the accuracy of soil erosion prediction on steep areas [30]. McCool et al. proposed an algorithm for calculating the slope factor using a piecewise function and included it in the RUSLE model [31] while Chinese researchers later modified the algorithm of slope factor for slopes above 10° using measured data, which has been widely used in the context of China [32]. However, most of the algorithms were based on measurements obtained from runoff plots below 15° , which may result in less accurate soil erosion prediction on steep areas. Therefore, it is important to improve the slope factor calculation, in order to improve the accuracy of soil erosion prediction, particularly in the areas with high slopes [33]. In this study, we obtained the fitting formula in the form of piecewise function that describes the functional relationship between the sine of slope θ and the slope factor, using the measured soil erosion data with the slopes ranging from 10 to 25° and above 25° .

Soil erodibility is also a key factor related to soil erosion estimation. Among many soil erodibility factor algorithms is the widely used Erosion Productivity Impact Calculator (EPIC) proposed by Williams et al. [34]. However, application of this algorithm to multiple erosion-prone areas of China resulted in soil erodibilities that were greater than measured values for all soil types [35]. This suggests that the EPIC algorithm might not be well suited for soil erodibility estimation in the context of China. Gravel on the soil surface or the top layer of soil has a direct or indirect effect on soil erosion [36]. A series of laboratory-based and runoff plot-based experiments show that rock fragment and gravel content are negatively related to soil erodibility [37–40]. Therefore, it is necessary to modify the prediction of soil erodibility. For improved soil erodibility estimation accuracy, gravel content, an important parameter used to modify the calculation of soil erodibility, should be considered in the RUSLE model. For the purpose of improving the accuracy of soil erodibility estimation, Shi [41] proposed a new algorithm to modify soil erodibility and constructed a piecewise function between relative soil erosion (ratio of soil erosions with different gravel content under the same condition) and gravel content. However, this algorithm has not been tested and applied in soil erodibility and soil erosion studies. In this study, this algorithm was used to modify the soil erodibility for the first time, and then we evaluated its accuracy and estimated soil erosion. China has been tackling soil erosion for decades in the Loess Plateau [42]. However, such an eco–environmental issue also occurs in many other areas, such as the Chaohu Lake Basin (CLB). In recent years, the contradiction between economic development, population, resources, and the eco–environment has become increasingly prominent in this region [43]. The decline of the eco–environmental quality in the CLB, such as eutrophication and increased soil erosion, has

seriously affected the sustainability of regional development. It is interesting that the mountainous areas in the eastern part of the CLB have high gravel content, reaching more than 20% in certain places. In this study, we therefore selected the CLB as the study area and used the RUSLE model for soil erosion estimation to contribute to the general goal of water and soil conservation. Specific objectives are as follows:

- (1) to modify the algorithms of calculating slope factor and soil erodibility factor in the RUSLE model for estimating the soil erosion in the CLB in 2017;
- (2) to examine the spatial distribution of each RUSLE factor over the study area;
- (3) to compare the soil erosion estimation results with and without modifying the soil erodibility algorithms.

2. Materials and Methods

2.1. Study Area

At the center of the east Chinese province of Anhui (116°20′–118°0′ E, 29°01′–33°16′ N), the CLB consists of 11 administrative districts—2 urban districts and 9 counties—covering a geographical area of $2.04 \times 10^4 \text{ km}^2$ (Figure 1). In 2017, the CLB had a population of around 11.52 million, with an urbanization rate of 68.5%, and produced a GDP of approximately 8345 billion CNY (Chinese yuan), according to the Statistical Yearbook of Anhui Province. Among the many water systems in the CLB is the Chaohu Lake, which is profiled as one of the five largest freshwater lakes in China, is one of the main drinking water sources in the CLB, and is replenished by surface runoff and rainfall. With an average elevation of 50.35 m, the CLB features highlands in the southwest and lowlands in the northeast. Influenced by geomorphic types and parent materials, the soil types in the CLB are particularly complex. The rainfall is mainly concentrated in summer and autumn, which accounts for more than 60% of the total annual rainfall, according to the rainfall data provided by the National Meteorological Information Center.

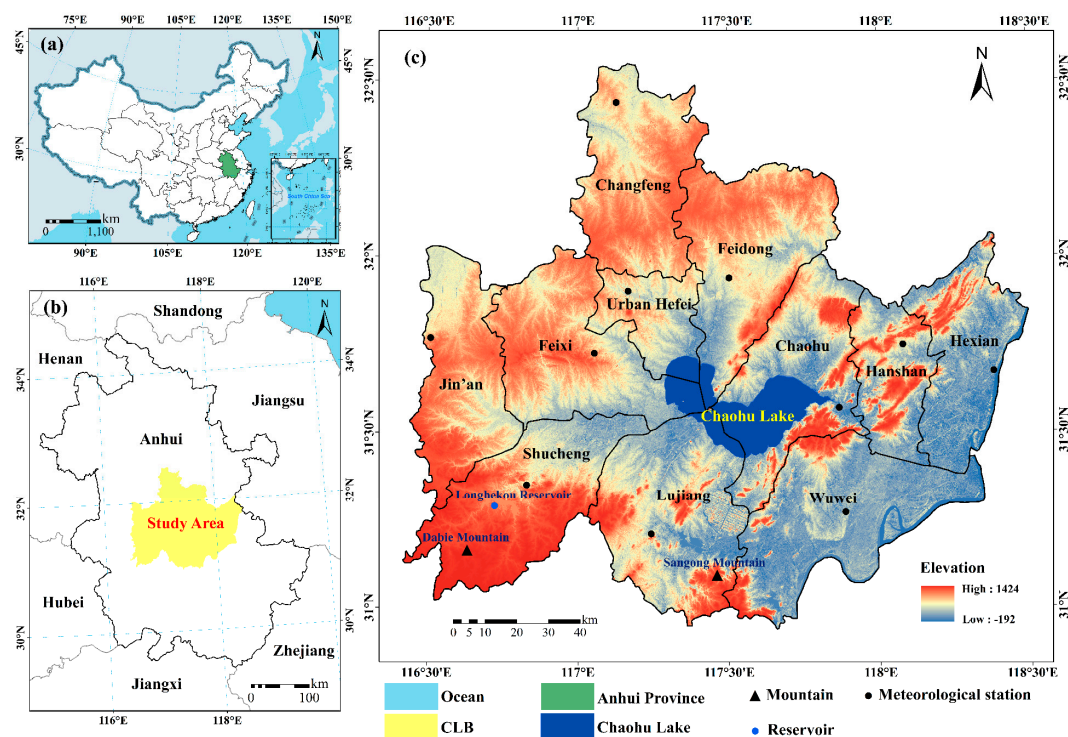


Figure 1. The study area: (a) the location of Anhui province in China; (b) the location of the Chaohu Lake Basin (CLB) in Anhui province; (c) the digital elevation model (DEM) of the CLB.

2.2. Data

Remote sensing images, digital elevation model (DEM) dataset, soil data, rainfall data, and vector data of the study area were used to generate the input variables for the RUSLE model (Table 1).

Table 1. Data used in this study.

Dataset	Description	Resolution	Source
Rainfall	Daily and monthly rainfall data of 13 meteorological stations from 1990 to 2017	0.05 degree	National Meteorological Information Center
Soil	Soil type and soil attribute data (subsoil sand fraction, silt fraction, clay fraction, topsoil organic carbon and gravel content)	1:1,000,000	Cold and Arid Regions Sciences Data Center at Lanzhou
DEM	ASTER GDEM dataset	30 m	Geospatial Data Cloud
Remote sensing imagery	Landsat 8 OLI (Operational Land Imager) data acquired on 21 July 2017 (Path120/Row38) and 28 July 2017 (Path121/Row38)	30 m	Geospatial Data Cloud
Vector	Provincial boundary	1:10,000	National Administration of Surveying, Mapping, and Geo-information

2.3. Methods

In this study, soil erosion was estimated using the RUSLE model, where the soil erodibility factor was modified by incorporating gravel content. The technical flowchart of this study is presented in Figure 2.

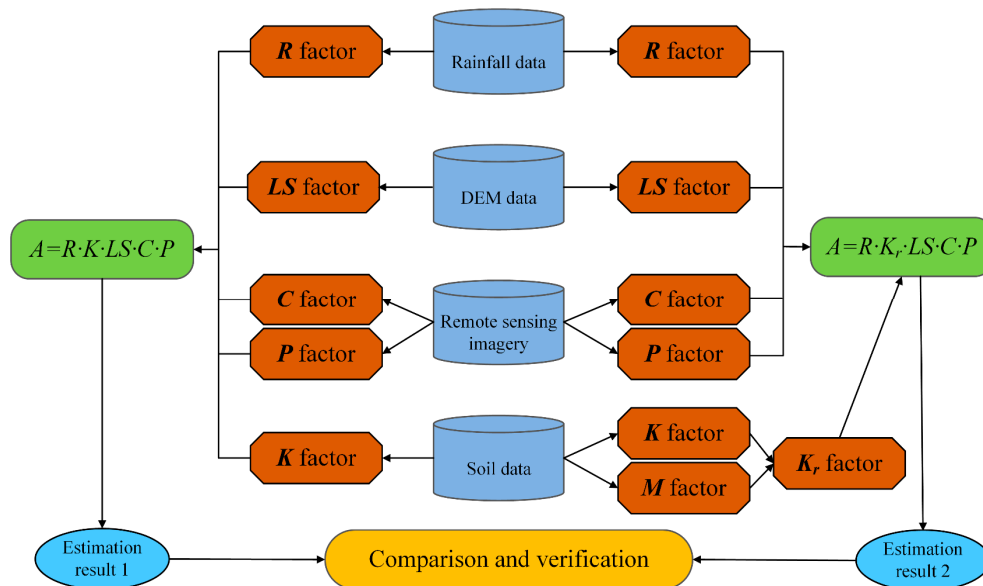


Figure 2. Flowchart depicting methodology of the study.

2.3.1. RUSLE

As a widely used soil erosion prediction model, the Revised Universal Soil Loss Equation (RUSLE) can quantify the soil erosion modulus in different scenarios and reflect the relationship between soil erosion and various impact factors [15]. Use of the RUSLE was made in this study based on the following equation [30,44]:

$$A = R \cdot K \cdot LS \cdot C \cdot P, \tag{1}$$

where A is the average annual soil loss ($\text{Mg}\cdot\text{ha}^{-1}\cdot\text{year}^{-1}$), R is the rainfall–runoff erosivity factor ($\text{MJ}\cdot\text{mm}\cdot\text{ha}^{-1}\cdot\text{hr}^{-1}\cdot\text{year}^{-1}$), K is the soil erodibility factor ($\text{Mg}\cdot\text{ha}\cdot\text{h}\cdot\text{ha}^{-1}\cdot\text{MJ}^{-1}\cdot\text{mm}^{-1}$), LS is the slope length and steepness factor (unitless) accounting the effect of topography on soil erosion, C is the cover fraction factor (unitless), and P is the support practice factor (unitless). These factors are detailed below.

- Rainfall–Runoff Erosivity Factor (R)

Rainfall erosivity is the potential possibility of soil erosion induced by rainfall, which is the most important external driving force and the dynamic indicator of soil separation and transportation [45,46]. Many of the existing classic and straightforward algorithms for estimating this factor are mainly based on annual rainfall, monthly, daily, or hourly rainfall [47–49]. Since using annual and monthly rainfall data results in less accurate estimation and it is often challenging to access hourly rainfall data, daily rainfall data was used in this study to calculate the rainfall erosivity in the CLB through the algorithm presented in the First National Census for Water [50]:

$$\bar{R}_k = \frac{1}{N} \sum_{i=1}^N \left(\alpha \sum_{j=1}^M P_{dikj}^\beta \right) \quad (2)$$

$$\alpha = 21.293\beta^{-7.3967}, \quad (3)$$

$$\beta = 0.6243 + \frac{27.346}{\bar{P}_{d_0}}, \quad (4)$$

$$\bar{P}_{d_0} = \frac{1}{N} \sum_{i=1}^N \sum_{k=1}^{12} \sum_{j=1}^M P_{dikj}, \quad (5)$$

$$\bar{R} = \sum_{k=1}^{12} \bar{R}_k, \quad (6)$$

where \bar{R}_k is the rainfall erosivity of the k th month ($\text{MJ}\cdot\text{mm}\cdot\text{ha}^{-1}\cdot\text{hr}^{-1}$), N is the sequence length of the calculated data; M is the frequency of erosive rainfall in the k th month of the i th year; P_{dikj} is the rainfall of the j th erosive rainfall in the k th month of the i th year (mm), and daily rainfall ≥ 12 mm is defined as erosive rainfall; α and β are model parameters calculated using Equations (3) and (4); \bar{P}_{d_0} is the multi-year average of erosive rainfall (mm); and \bar{R} is the average annual rainfall erosivity ($\text{MJ}\cdot\text{mm}\cdot\text{ha}^{-1}\cdot\text{hr}^{-1}\cdot\text{year}^{-1}$).

- Soil Erodibility Factor (K)

The soil erodibility factor K reflects the sensitivity of soil to erosion. The K value can be estimated by making observations at a large number of test plots; however, such an approach is difficult to apply to a large watershed [51,52] such as the CLB. To solve this issue, we calculated soil erodibility in this study based on the EPIC model [34] using the following equation:

$$K = \left\{ 0.2 + 0.3 \exp \left[-0.0256 W_d \left(1 - \frac{W_i}{100} \right) \right] \right\} \times \left(\frac{W_i}{W_i + W_l} \right)^{0.3} \times \left[1 - \frac{0.25 W_c}{W_c + \exp(3.72 - 2.95 W_c)} \right] \times \left[1 - \frac{0.7 W_n}{W_n + \exp(-5.51 + 22.9 W_n)} \right], \quad (7)$$

where W_d is the fraction of sand ($\phi 2\text{--}0.05$ mm) in %, W_i is the fraction of silt ($\phi 0.05\text{--}0.002$ mm) in %, W_l is the fraction of clay ($\phi < 0.002$ mm) in %, W_c is the soil total organic carbon content in %, and $W_n = 1 - \frac{W_d}{100}$.

- Slope Length and Steepness Factor (LS)

The slope length and steepness factor (LS) can accelerate soil erosion, representing the influence of topographic features on soil erosion [53]. A steeper slope and a longer slope length lead to more serious soil erosion [54]. The L value can be calculated by the following equation [55]:

$$L = (\text{cell size} / 22.13)^m, \quad (8)$$

where cell size = grid cell size (30 m in this study); the value of m varies between 0.2 and 0.5 (0.2 for slopes less than 1%, 0.3 for 1–3%, 0.4 for 3–4.5%, and 0.5 for slopes exceeding 4.5%).

As mentioned in the Introduction (Section 1), Wischmeier and Smith modified the relationship between soil erosion and slope by creating the slope factor S , which is the quadratic function of the sine of slope θ (Equation (9)) and applied it in the USLE (Universal Soil Loss Equation) model [30]:

$$S = 65.4 \sin^2 \theta + 4.56 \sin \theta + 0.0654. \quad (9)$$

Then, the slope factor formula was modified using observation data in the RUSLE model [32]:

$$S = \begin{cases} 10.8 \sin \theta + 0.03 & \theta \leq 5^\circ \\ 16.8 \sin \theta - 0.50 & 5^\circ < \theta \leq 10^\circ \\ 21.9 \sin \theta - 0.96 & \theta > 10^\circ \end{cases} \quad (10)$$

This algorithm improves the prediction accuracy of soil loss on slopes above 10° . However, it would not be appropriate for soil erosion estimation in the context of the CLB because soil erosion mainly occurs in mountainous and hilly areas with high slopes in the CLB [56]. As such, it would be necessary to modify this algorithm in the case of slopes greater than 10° . By extraction from scientific research articles, reports, and books, we compiled a dataset of measured soil erosion for a number of plots (see Table A1, Appendix A). This dataset covers slopes ranging from 10° to 45° , which are highly representative. We used these sample data to establish the functional relationship between the sine of slope θ and the slope factor.

- Cover Fraction Factor (C)

The C factor characterizes the restriction of surface vegetation cover on soil erosion as vegetation helps to retain soil and water [1]. Although both spectral vegetation indices and spectral mixture analysis modeled vegetation fractions [57–59] can be used to calculate the C factor values [60,61], it is easier to extract spectral vegetation indices than vegetation fractions. In this study, the mostly commonly used vegetation index, Normalized Difference Vegetation Index ($NDVI$), which is the ratio of the difference between spectral reflectance in near infrared and red regions [62,63], was used to calculate C factor values according to the following equation [64]:

$$C = \exp\left[-\alpha \cdot \frac{NDVI}{(\beta - NDVI)}\right], \quad (11)$$

where α and β are parameters that determine the shape of the $NDVI$ - C curve, and the α -value of 2 and β -value of 1 provide reasonable results of C values compared with those estimated as summing a linear relationship [65].

- Support Practice Factor (P)

The P factor is defined as the ratio of soil loss with a specific support practice to the corresponding loss with upslope and downslope tillage [66]. It is a dimensionless factor with a value between 0 and 1 [44]: 0 means that no soil erosion will occur while 1 means that no soil and water conservation measures have been taken or the measures have completely failed. The P factor is closely related to land use type and land use change [67]. Using the maximum likelihood classifier, we classified the land

use/cover types in the CLB into six categories, namely farmland, forestland, grassland, water body, construction land, and unused land. The high-resolution satellite images in 2017 provided by Google Earth Pro were used to assess classification accuracy [68]. In total, 500 sample points were randomly generated in the classified image in ArcGIS 10.1 and then imported into Google Earth Pro to retrieve the ground-truthing data. By constructing a confusion matrix, we obtained the overall accuracy (90.1%) and Kappa coefficient (0.86) for this classification. These high values indicate that the classification was well performed and that the classification map could be used for further analysis in this study.

In this study, we used the land use classification of the CLB in 2017 (Figure 3) and assigned the *P* factor values from Zha et al. [56] and Xu et al. [4] for each land use type (Table 2).

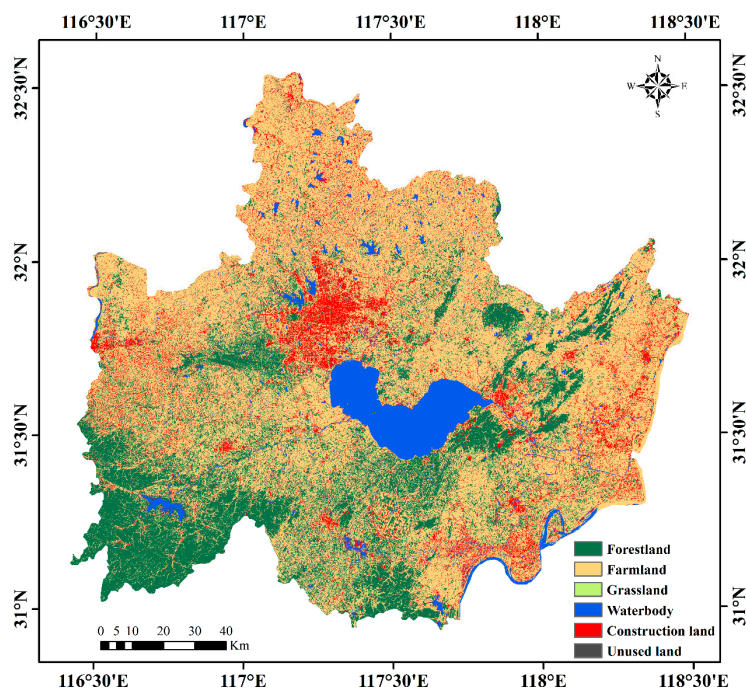


Figure 3. Land use classification map of the CLB in 2017.

Table 2. The *P* factor value of different land use types.

Land Use Type	Farmland	Forestland	Grassland	Waterbody	Construction Land	Unused Land
<i>P</i> factor value	0.35	1	1	0	0	1

2.3.2. Modifying Soil Erodibility (*K*)

In order to modify soil erodibility, gravel content was considered as a key parameter. The piecewise function proposed by Shi [41] was used for the first time to modify soil erodibility, which describes the functional relationship between relative soil erosion and different gravel content ranges. The modification coefficient *M* (relative soil erosion) was determined by the following equation:

$$M = \begin{cases} 0.0781e^{-0.0249R_m} & R_m > 20\% \\ 0.294 - 0.0123R_m & 10\% < R_m \leq 20\%, \\ 1 - 0.0829R_m & R_m \leq 10\% \end{cases} \quad (12)$$

where *M* is the coefficient for modifying the soil erodibility, and *R_m* is the gravel content. The modified soil erodibility can be obtained by the following equation:

$$K_r = K \times M, \quad (13)$$

where K_r is the modified soil erodibility ($\text{Mg}\cdot\text{ha}\cdot\text{h}\cdot\text{ha}^{-1}\cdot\text{MJ}^{-1}\cdot\text{mm}^{-1}$), and K is the soil erodibility calculated by the EPIC model ($\text{Mg}\cdot\text{ha}\cdot\text{h}\cdot\text{ha}^{-1}\cdot\text{MJ}^{-1}\cdot\text{mm}^{-1}$). Using Equations (7), (12), and (13), the soil erodibility K and the modified soil erodibility K_r can be calculated. In order to assess the accuracy of this modified algorithm, five sets of measured soil erodibility data extracted from Zhang et al. [35] were used to compare with our modified soil erodibility.

3. Results

3.1. Fitting Equation of Slope Factor

Using the measured soil erosion dataset, we obtained the fitted equation with high confidence level between slope factor and sine value in the ranges of 10° – 25° and above 25° , respectively. The regression analysis shown in Figure 4 shows a strong linear relationship between them.

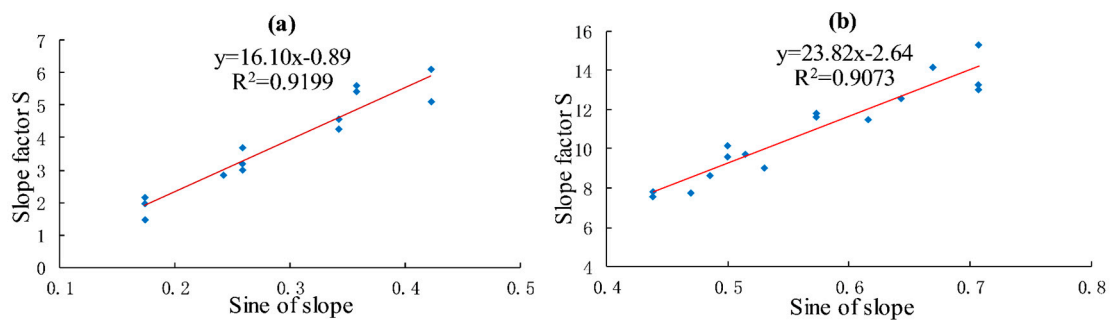


Figure 4. Relationship between the sine of slope and the slope factor: (a) slopes between 10° and 25° ; and (b) slopes above 25° .

As such, based on the algorithm proposed by Liu et al. [33], the estimation of slope factor in the case of slopes higher than 10° can be calculated by the following equation:

$$S = \begin{cases} 10.8 \sin \theta + 0.03 & \theta \leq 5^\circ \\ 16.8 \sin \theta - 0.50 & 5^\circ < \theta \leq 10^\circ \\ 16.10 \sin \theta - 0.89 & 10^\circ < \theta \leq 25^\circ \\ 23.82 \sin \theta - 2.64 & \theta > 25^\circ \end{cases} \quad (14)$$

3.2. Accuracy Assessment of Modified Soil Erodibility

The calculated K values and K_r values were shown in Figure 5. We found that the range of the original K values was smaller than that of the modified soil erodibility K_r values. The means of modified soil erodibility K_r were remarkably reduced. This suggests that gravel content has an important effect on the calculation of soil erodibility.

It is clear that the measured K values for the five types were all within the range of K_r (Table 3). By comparing the ratios of the calculated K and K_r values to the measured values, we noticed that the calculated K_r values were by far closer to the measured values than the calculated K values. It is therefore believed that this modified algorithm can result in better soil erodibility estimation and has the potential to improve the accuracy of soil erosion prediction.

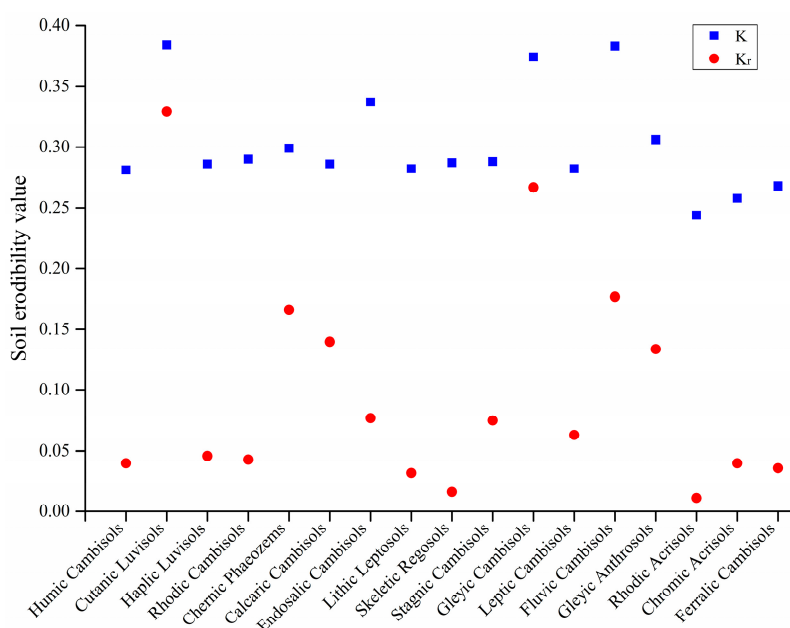


Figure 5. The K values and K_r values for each soil types.

Table 3. Comparison of calculated and measured soil erodibility.

Soil Type	Mean of Gravel Content (%)	Mean of K	Mean of K _r	Measured Value	R ₁	R ₂
Skeletal Regosols	21.9	0.29	0.02	0.01	20.5	1.1
Chernic Phaeozems	4.6	0.30	0.17	0.29	1.03	0.6
Endosalic Cambisols	9.5	0.31	0.08	0.15	2.3	0.5
Rhodic Acrisols	22.5	0.24	0.01	0.01	17.4	0.8
Haplic Luvisols	10.9	0.29	0.05	0.07	3.9	0.6

Note: ¹ R₁ is the ratio of the mean of K to the measured value and R₂ is the ratio of the mean of K_r to the measured value.

With the modified algorithm of soil erodibility factor, the RUSLE model (Equation (1)) can be transformed as follow:

$$A = R \cdot K_r \cdot LS \cdot C \cdot P. \tag{15}$$

3.3. RUSLE Factors

The R values in the CLB varied from 2856.17 to 8985.13 MJ·mm·ha⁻¹·hr⁻¹·year⁻¹, with a mean of 4244.71 MJ·mm·ha⁻¹·hr⁻¹·year⁻¹ (Figure 6a). Spatially, the values decreased from southwest to northeast with the highest and smallest values of R observed in the counties of Shucheng and Feixi, respectively.

The K_r value obtained by Equation (13) varied from 0 to 0.38 Mg·ha·h·ha⁻¹·MJ⁻¹·mm⁻¹ (Figure 6b). Accounting for 67.9% of the basin’s area, gleyic anthrosols was characterized by soil erodibility values ranging between 0.25 and 0.28 Mg·ha·h·ha⁻¹·MJ⁻¹·mm⁻¹. The K_r values for ferralic cambisols, endosalic cambisols, lithic leptosols, skeletal regosols, and stagnic cambisols were nearly equal to 0. The soil types with the highest K_r value were the humic cambisols (0.36 Mg·ha·h·ha⁻¹·MJ⁻¹·mm⁻¹) and calcareic cambisols (0.38 Mg·ha·h·ha⁻¹·MJ⁻¹·mm⁻¹), mainly distributed in the Dabie Mountains in the southwest, the Sangong Mountains in the south, Chaohu east of Chaohu Lake, and mountainous areas in Hanshan.

The LS value in the CLB changed from 0.03 to 40.57, with a mean of 1.04 (Figure 6c). The areas with LS values > 5 were mainly concentrated in the mountainous areas with high elevations and slopes, while the areas with LS values < 0.1 were mostly distributed in flat terrain that was dominated by construction land and lakes.

The C value in the CLB varied from 0 to 1, with a mean of 0.73 (Figure 6d). When the C value = 1, it represents invalid vegetation cover and management measures and a low NDVI value,

with a high probability of soil erosion; conversely, when the C value = 0, it represents vegetation cover and management measures to inhibit soil erosion with a positive effect. The calculation of C value in the CLB shows that the vegetation cover was concentrated in the areas with low C value.

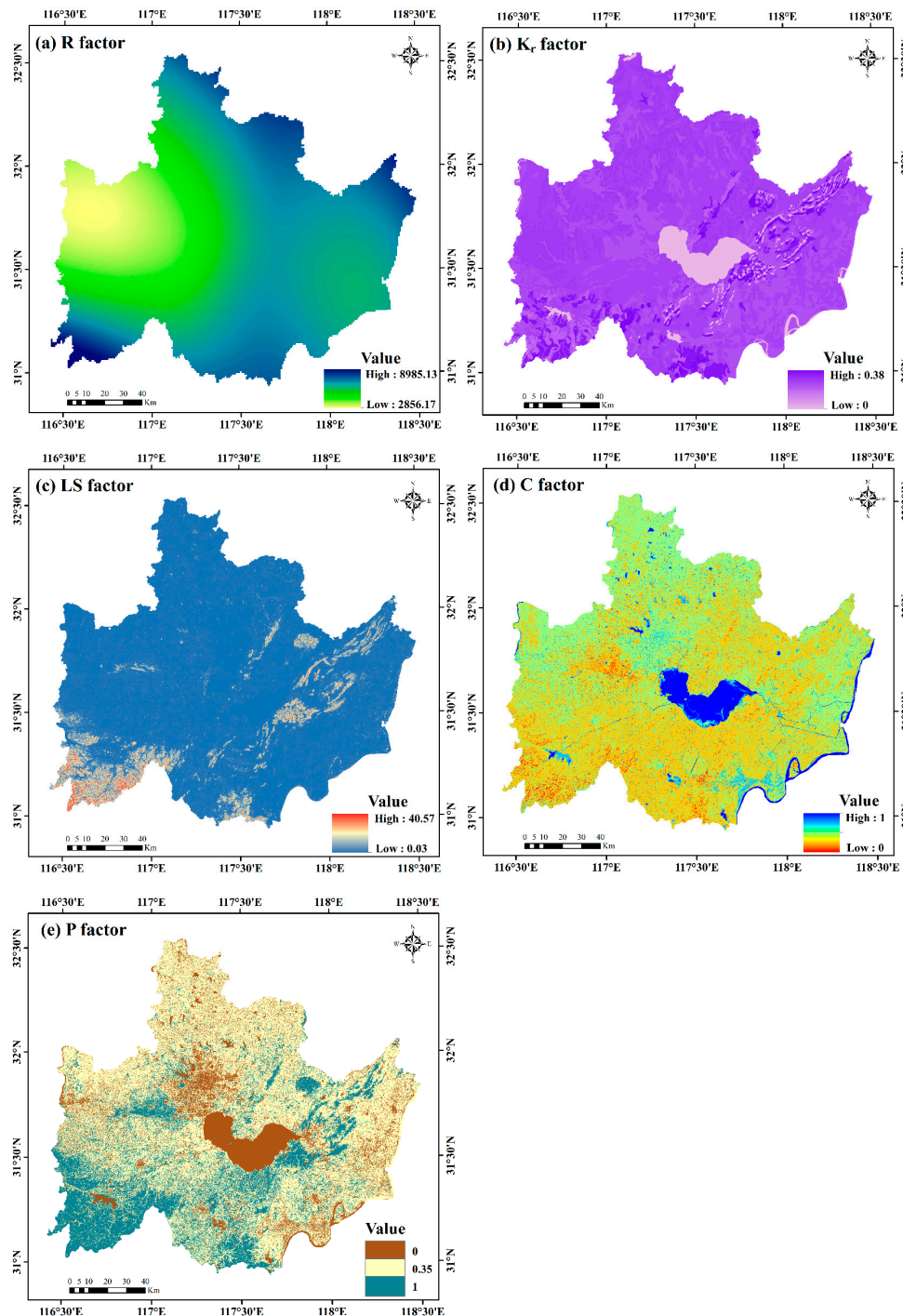


Figure 6. Maps of the Revised Universal Soil Loss Equation (RUSLE) factors: (a) R , the rainfall–runoff erosivity factor; (b) K_r , the soil erodibility factor; (c) LS , the slope length and steepness factor; (d) C , the cover fraction factor; (e) P , the support practice factor.

The results of land use/cover classification (Section 2.3.1) show that the farmland area was 1,196,187 km² (accounting for 58.7% of the basin area), which is the largest land use type in the CLB. The forestland area reached 4490.87 km² (22%) and the construction land area was 2157.64 km² (10.6%).

The areas of water body, grassland, and unused land were relatively small, comprising only 6.9%, 0.1%, and 1.8%, respectively. The P value was as signed according to the land use/cover classification results, varying from 0 to 1 (Figure 6e). It is shown that the areas with large P factor values were concentrated in the mountainous area and its surrounding area. Areas with small P factor values were mainly concentrated in construction land, water body, and unused land, where we assume that the probability of their soil erosion is low.

3.4. Soil Erosion Estimation

With the factors calculated above, we used the RUSLE in the form of Equations (1) and (15) to estimate the soil erosion of the CLB in 2017. In order to show the differences between soil erosion estimation results clearly, estimated soil erosion was divided into six grades according to the Standards for Classification and Gradation of Soil Erosion issued by the Ministry of Water Resources of the People's Republic of China (SL190-2007) [69]: slight ($<5 \text{ Mg}\cdot\text{ha}^{-1}\cdot\text{year}^{-1}$), light ($5\text{--}25 \text{ Mg}\cdot\text{ha}^{-1}\cdot\text{year}^{-1}$), moderate ($25\text{--}50 \text{ Mg}\cdot\text{ha}^{-1}\cdot\text{year}^{-1}$), intense ($50\text{--}80 \text{ Mg}\cdot\text{ha}^{-1}\cdot\text{year}^{-1}$), extremely intense ($80\text{--}150 \text{ Mg}\cdot\text{ha}^{-1}\cdot\text{year}^{-1}$), and severe ($>150 \text{ Mg}\cdot\text{ha}^{-1}\cdot\text{year}^{-1}$). The grading maps are shown in Figure 7.

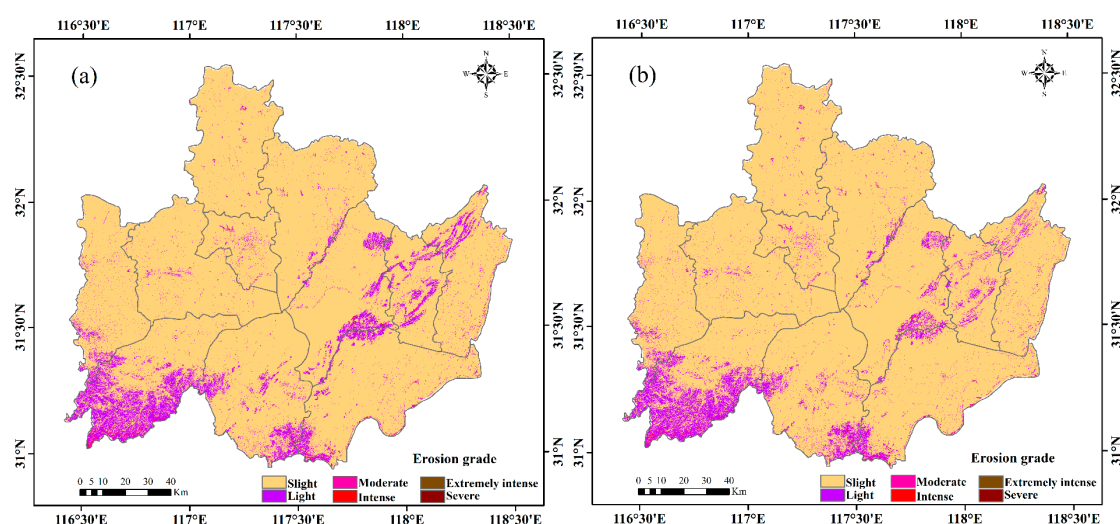


Figure 7. Soil erosion grading maps of the CLB: (a) soil erosion modulus estimated from Equation (1); and (b) soil erosion modulus estimated from Equation (15).

As seen in Table 4, the two equations resulted in different soil erosion moduli and our estimation ($1.78 \text{ Mg}\cdot\text{ha}^{-1}\cdot\text{year}^{-1}$ by Equation (15)) was slightly lower than the original RUSLE ($1.92 \text{ Mg}\cdot\text{ha}^{-1}\cdot\text{year}^{-1}$ by Equation (1)). Both calculation results showed that Shucheng was the largest contributor ($\sim 5 \text{ Mg}\cdot\text{ha}^{-1}\cdot\text{year}^{-1}$) to soil loss in the CLB. In contrast, smallest soil erosion moduli were observed in Changfeng, Feidong, and Feixi, all lower than $1 \text{ Mg}\cdot\text{ha}^{-1}\cdot\text{year}^{-1}$. The comparison also revealed that there was almost no change in the average annual soil erosion modulus for Changfeng, Jin'an, Urban Hefei, Feidong, and Feixi while the estimation from Equation (15) was lower than that from Equation (1) for the rest of the districts and counties.

In addition, we compared the measured data of 11 districts in the CLB provided by Anhui Provincial Water Conservancy Station with the results of Equations (1) and (15) (Figure 8). It can be observed that all the measured data were smaller than the result of Equation (1), where the largest difference was $0.59 \text{ Mg}\cdot\text{ha}^{-1}\cdot\text{year}^{-1}$ in Shucheng and the smallest difference was $0.11 \text{ Mg}\cdot\text{ha}^{-1}\cdot\text{year}^{-1}$ in Changfeng. In general, the result of Equation (15) was closer to the measured data than that of Equation (1). The largest difference between the result of Equation (15) and the measured data was $0.44 \text{ Mg}\cdot\text{ha}^{-1}\cdot\text{year}^{-1}$ in Shucheng and the smallest difference was $0.08 \text{ Mg}\cdot\text{ha}^{-1}\cdot\text{year}^{-1}$ in Hexian, both smaller than those for Equation (1). Figure 8 also shows that the differences between the results of

Equations (1) and (15) with the measured data were the same in Changfeng, Jin'an, Urban Hefei, Feidong, and Feixi. For the entire study area, the differences between the two results and the measured data were $0.26 \text{ Mg}\cdot\text{ha}^{-1}\cdot\text{year}^{-1}$ for the result of Equation (1) and $0.12 \text{ Mg}\cdot\text{ha}^{-1}\cdot\text{year}^{-1}$ for the result of Equation (15).

Table 4. Average soil erosion modulus of the CLB in 2017 ($\text{Mg}\cdot\text{ha}^{-1}\cdot\text{year}^{-1}$).

Area	Equation (1)	Equation (15)	Differences
CLB	1.92	1.78	-0.14
Wuwei	1.89	1.72	-0.17
Changfeng	0.96	0.96	0.00
Jin'an	1.58	1.57	-0.01
Urban Hefei	1.32	1.32	0.00
Feidong	0.98	0.98	0.00
Feixi	0.96	0.96	0.00
Shucheng	5.10	4.95	-0.15
Lujiang	2.07	1.98	-0.09
Chaohu	1.80	1.47	-0.33
Hanshan	2.44	1.80	-0.64
Hexian	1.67	1.36	-0.31

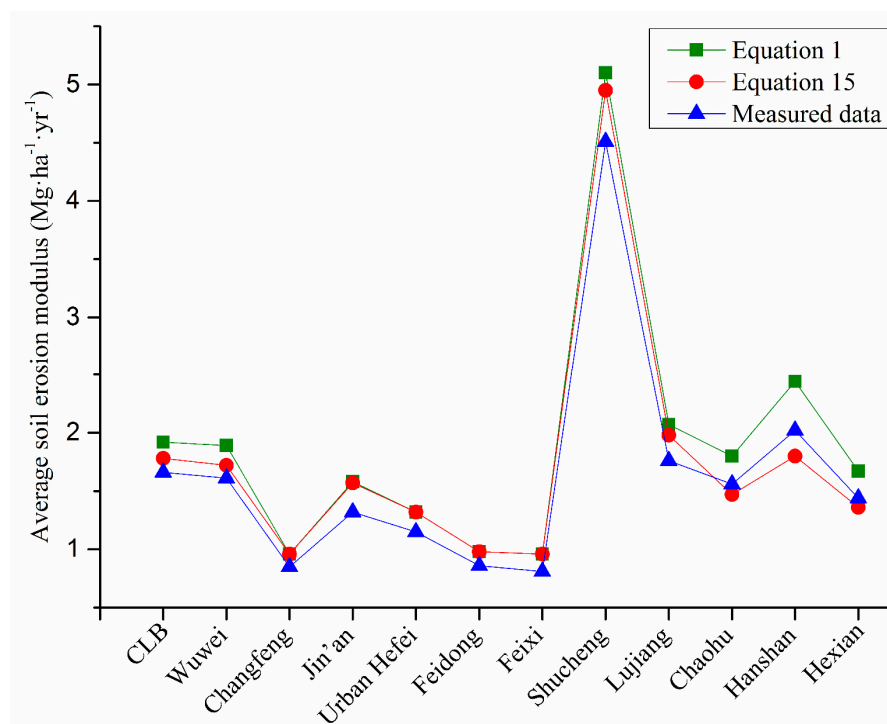


Figure 8. Comparison of the results of Equations (1) and (15) with the measured data.

Table 5 shows the areas and proportions of each soil erosion grade. The area for each grade was quite similar from the two estimations. It is clear that the erosion-affected area (from slight to severe level) in the CLB in 2017 was $19,087.35 \text{ km}^2$, accounting for 93.6% of the total area. The slight level was the largest (~85%) among all the levels, followed the light level (~8%). The areas of intense and extremely intense levels were quite small, both composing less than 1%. Despite a large erosion-affected area, there was no severe-level soil erosion in the CLB.

Table 5. Area for each soil erosion grade.

Grade	Equation (1)		Equation (15)	
	Area (km ²)	Proportion (%)	Area (km ²)	Proportion (%)
No erosion	1303.08	6.39	1303.08	6.39
Slight	17,266.30	84.66	17,445.76	85.55
Light	1686.46	8.27	1531.47	7.51
Moderate	116.24	0.57	97.88	0.48
Intense	14.27	0.07	10.20	0.05
Extremely intense	4.08	0.02	4.08	0.02
Severe	0.00	0.00	0.00	0.00

Figure 9 shows the soil erosion grade for each district and county of the CLB; the slight level was the largest at over 60% for each part of the CLB. Shucheng had more light-erosion (>30%) and moderate-erosion (>2%) areas than the other 10 districts and counties. While Wuwei, Shucheng, and Chaohu had the largest intense erosion areas, no extremely intense erosion was estimated in Changfeng, Jin’an, Urban Hefei, Feidong, and Feixi. Figure 9 also reveals that the two estimations resulted in quite similar distributions of soil erosion grades in these districts, except for the intense level for Hanshan (Figure 9d) and the extremely intense level for Chaohu (Figure 9e).

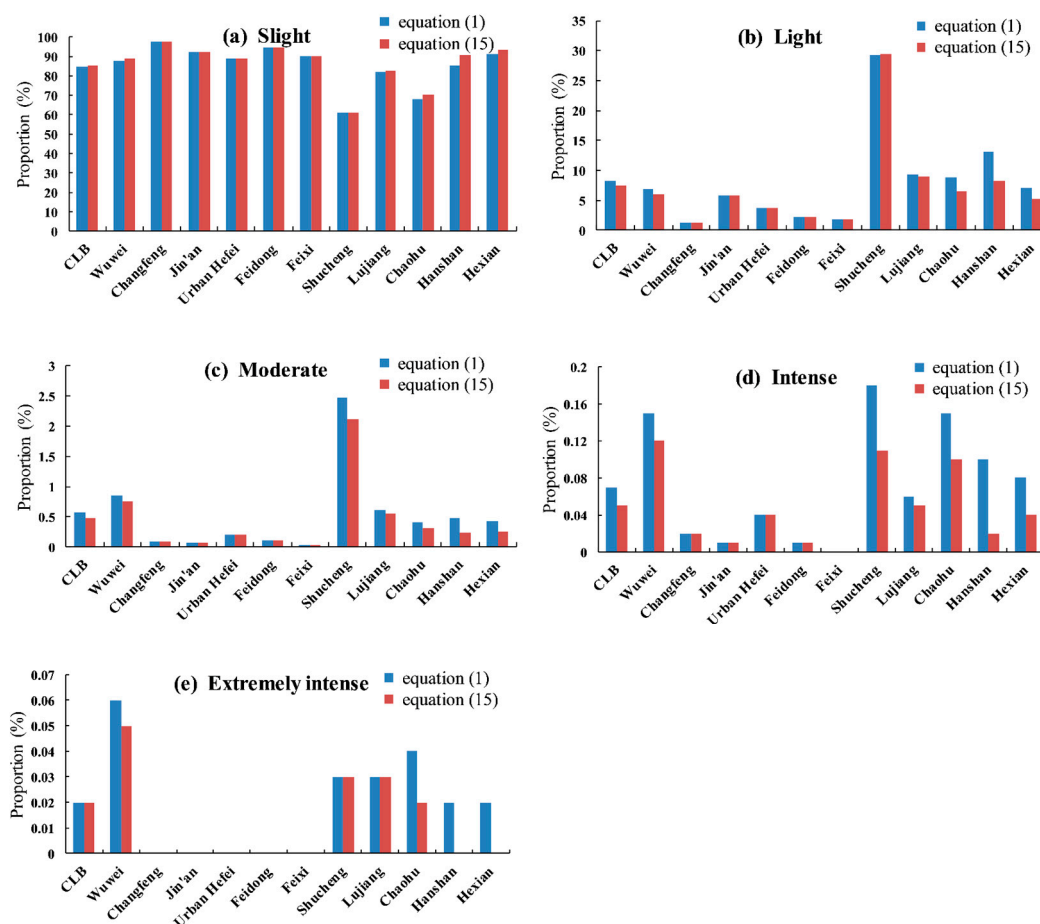


Figure 9. The distribution of soil erosion grade in the CLB and its 11 districts and counties: (a) Slight; (b) Light; (c) Moderate; (d) Intense; and (e) Extremely intense.

4. Discussion

In this study, we estimated the soil erosion in the CLB in 2017 using the original RUSLE model and the RUSLE model with modified soil erodibility. In addition, the distribution of soil erosion grades in the CLB and its 11 administrative districts were investigated. The interpretation of the results and their implications are given in this section.

4.1. Factors of the RUSLE Model

Soil erosion is a complex process influenced by a variety of natural and human-induced factors [70]. Five factors are considered to estimate soil erosion in the RUSLE model [71,72], namely rainfall erosivity (R), soil erodibility (K), slope length and steepness (LS), cover fraction (C), and support practice (P). The R factor, K factor, and LS factor contribute to greater soil erosion [4] while the C factor and P factor play an important role in preventing soil erosion [27]. By comparing the maps of the R factor, K factor, and LS factor (Figure 6) and the estimated soil erosion (Figure 7), we notice that the three factors are highly consistent with soil erosion in spatial distribution. This helps to explain why soil erosion was higher in Wuwei, Shucheng, Lujiang, Chaohu, Hanshan, and Hexian than the other parts of the CLB. Similarly, Figure 6 shows that the C factor and P factor play an irreplaceable role in the control of soil erosion, especially in the areas with topographic fluctuation. Since it is difficult to change the natural factors such as rainfall, topography, and soil properties, optimizing land use structure and improving vegetation coverage are considered the most effective measures to prevent soil erosion [18].

4.2. Influence of Gravel Content on Soil Erosion Estimation

Based on the comparison of the results of Equations (1) and (15) with the measured data, we found that all the calculated soil erosion modulus combined with the modified soil erodibility were closer to the measured data in Wuwei, Shucheng, Lujiang, Chaohu, Hanshan, and Hexian, which are characterized by mountainous area with high gravel content. However, there were no differences between the two results with the measured data in the districts with small mountainous areas, such as Changfeng, Jin'an, Urban Hefei, Feidong, and Feixi. Therefore, we consider that the accuracy of soil erodibility has an important impact on soil erosion estimation [73,74]. The K values calculated by the method in the RUSLE model were much larger than the measured values. In this study, the gravel content parameter was added into the modified algorithm for soil erodibility, and the estimated K_r values were closer to the measured ones. The accuracy of soil erosion estimation in the CLB was accordingly effectively improved using the modified soil erodibility. Therefore, we believe that this might be because the effect of gravel content on soil erosion was not fully considered.

Many previous studies about the effect of rock fragment and gravel content on soil erosion have also reached similar conclusions. Rodrigo-Comino et al. [37] carried out an investigation with 96 rainfall simulation experiments at the pedon scale and found that the soil losses are inversely proportional to rock fragment cover on the soil surface. Cerdà [38] carried out 20 experiments on bare areas of natural soils and the results showed that water and soil losses were reduced by the rock fragments. Poesen et al. [39] have reported the various effects of rock fragments on soil erosion and the key finding shows that rock fragment cover will offer protection to topsoil and have different efficiencies in different nested spatial scales. The results of two laboratory flume experiments carried out by Jomaa et al. [40] revealed that the rock fragments decreased the sediment transport capacity. These studies provide a reliable support for our views.

4.3. Characteristics of Soil Erosion in the CLB

Overall, the erosion-affected areas of the CLB were mainly distributed along the SW–NE direction. While the slight-level soil erosion was mostly found in the alluvial plains along the middle and lower reaches of the Nanfei River, Hangbu River, and Tianhe River, and the low mountain and hilly areas with high vegetation coverage (Figure 7), the areas with high soil erosion modulus in the CLB concentrated

in the northeast of Dabie Mountain, the north of Sangong Mountain, and the mountainous areas of Chaohu and Hanshan. Particularly, the population density of Longhekou Reservoir area in Shucheng was high and inappropriate land use existed in this area, such as steep slope reclamation and excessive vegetation destruction. The intensive interaction between human and nature has caused reservoir siltation, thus serious soil erosion problems [75].

4.4. Limitations

Soil erosion estimation is a key to the understanding and management of the ecological environment, particularly in ecologically vulnerable regions [76]. Although it is considered as a widely used approach to soil erosion estimation [74,77], the application of the RUSLE model might be region-specific due to the complexity of the ecological environment [23]. In the case study of the CLB, the gravel content parameter was used to modify the algorithm of soil erodibility factor in the RUSLE model. Such revision has proved to improve soil erosion estimation for the CLB. Despite the improvement, there are some issues that should be addressed in further research:

- (1) the accuracy of soil erodibility obtained by the modified algorithm using the gravel content was assessed based on only five soil types and an exhaustive assessment is required; and
- (2) due to the limitation of data acquisition, only 13 meteorological stations could provide rainfall data to estimate rainfall erosivity, which might reduce the accuracy of rainfall erosivity estimation.

5. Conclusions

We estimated and compared the soil erosion of the Chaohu Lake Basin (CLB) in 2017 using the original RUSLE model and the RUSLE model with modified soil erodibility. The average annual soil erosion estimated with the K_r algorithm was $0.14 \text{ Mg}\cdot\text{ha}^{-1}\cdot\text{year}^{-1}$ lower than the estimation result with the original K algorithm in the CLB. In other words, taking gravel content into account helps to improve the calculation of soil erodibility and soil erosion estimation. The overall soil erosion in the CLB was low with a majority of slight erosion (accounting for 85.6%), and the mountainous and hilly areas are more prone to soil erosion. The superposition of inappropriate land use and natural factors (including climate, soil properties, and topography) is the main reason for soil erosion of the CLB and should be optimized for soil erosion prevention in the CLB.

Quantitative analysis of soil erosion is highly beneficial in natural resource management and policy-making to relieve the pressure of soil erosion and land degradation. The findings of this study provide useful insights into the spatial distribution of soil erosion and the driving mechanism in this ecologically important region.

Author Contributions: Conceptualization, S.H. and L.L.; methodology, S.H.; software, L.C. (Liang Cheng) and L.Y.; validation, S.H. and X.H.; formal analysis, S.H.; data curation, X.H. and T.Z.; writing—original draft preparation, S.H.; writing—review and editing, L.L. and L.C. (Longqian Chen); visualization, S.H.; supervision, project administration, and funding acquisition, L.C. (Longqian Chen). All the authors reviewed and approved the final manuscript version.

Funding: This research was funded by the Fundamental Research Funds for the Central Universities under grant number 2018ZDPY07.

Acknowledgments: The authors thank the Geospatial Data Cloud for freely providing the Landsat data, the Cold and Arid Regions Sciences Data Center for the soil data, and the National Meteorological Information Center for the rainfall data. Furthermore, we appreciate the editors and reviewers for their constructive comments and suggestions.

Conflicts of Interest: The authors declare no conflict of interest.

Appendix A

Table A1. Measured soil erosion dataset.

Slope Gradient (°)	Land Use	Soil Loss Rate (Mg·ha ⁻¹ ·yr ⁻¹)	Reference
15°	arable land	198.2	Yang [78]
15°	arable land	234.64	Yang [78]
21°	arable land	366.12	Yang [78]
21°	arable land	432.14	Yang [78]
29°	arable land	474.04	Yang [78]
42°	arable land	865.88	Yang [78]
45°	arable land	991.48	Yang [78]
45°	arable land	897.58	Yang [78]
45°	arable land	958.22	Yang [78]
10°	bare	83.9	Mu [79]
15°	bare	120.5	Mu [79]
20°	bare	136.21	Mu [79]
25°	bare	210.5	Mu [79]
30°	bare	272.71	Mu [79]
40°	bare	308.08	Mu [79]
10°	arable land	44.21	Bi [80]
20°	arable land	103.26	Bi [80]
25°	shrub	139.87	Bi [80]
28°	shrub	140.7	Bi [80]
32°	bare	103.24	Tang et al. [81]
35°	bare	152.86	Tang et al. [81]
38°	bare	217.74	Tang et al. [81]
30°	bare	83.65	Zhang [82]
35°	bare	100.12	Zhang [82]
10°	grassland	355.19	Xu et al. [83]
14°	arable land	38.4	Wang [84]
26°	fallow	214.62	Lin [85]
26°	arable land	35.39	Wu et al. [86]
31°	fallow	92.66	Liu et al. [87]

References

1. Patowary, S.; Sarma, A.K. GIS-based estimation of soil loss from hilly urban area incorporating hill cut factor into RUSLE. *Water Resour. Manag.* **2018**, *32*, 3535–3547. [[CrossRef](#)]
2. Zhao, J.; Vanmaercke, M.; Chen, L.; Govers, G. Vegetation cover and topography rather than human disturbance control gully density and sediment production on the Chinese Loess Plateau. *Geomorphology* **2016**, *274*, 92–105. [[CrossRef](#)]
3. Rahman, M.R.; Shi, Z.H.; Chongfa, C. Soil erosion hazard evaluation—An integrated use of remote sensing, GIS and statistical approaches with biophysical parameters towards management strategies. *Ecol. Model.* **2009**, *220*, 1724–1734. [[CrossRef](#)]
4. Xu, L.; Xu, X.; Meng, X. Risk assessment of soil erosion in different rainfall scenarios by RUSLE model coupled with Information Diffusion Model: A case study of Bohai Rim, China. *Catena* **2012**, *100*, 74–82. [[CrossRef](#)]
5. Pimentel, D. Soil erosion: A food and environmental threat. *Environ. Dev. Sustain.* **2006**, *8*, 119–137. [[CrossRef](#)]
6. Park, S.; Jeon, S.; Choi, C.; Oh, C.; Jung, H. Soil erosion risk in Korean watersheds, assessed using the revised universal soil loss equation. *J. Hydrol.* **2011**, *399*, 263–273. [[CrossRef](#)]
7. Vrieling, A.; de Jong, S.M.; Sterk, G.; Rodrigues, S.C. Timing of erosion and satellite data: A multi-resolution approach to soil erosion risk mapping. *Int. J. Appl. Earth Obs. Geoinf.* **2008**, *10*, 267–281. [[CrossRef](#)]
8. Montanarella, L. Agricultural policy: Govern our soils. *Nature* **2015**, *528*, 32–33. [[CrossRef](#)]

9. Rodrigo-Comino, J.; Keesstra, S.; Cerdà, A. Soil erosion as an environmental concern in vineyards: The case study of Celler del Roure, eastern Spain, by means of rainfall simulation experiments. *Beverages* **2018**, *4*, 31. [[CrossRef](#)]
10. Rodrigo-Comino, J.; Davis, J.; Keesstra, S.D.; Cerdà, A. Updated measurements in vineyards improves accuracy of soil erosion rates. *Agron. J.* **2017**, *110*, 411–417. [[CrossRef](#)]
11. Cerdà, A.; Ackermann, O.; Terol, E.; Rodrigo-Comino, J. Impact of farmland abandonment on water resources and soil conservation in citrus plantations in eastern Spain. *Water* **2019**, *11*, 824. [[CrossRef](#)]
12. Cerdà, A.; Rodrigo-Comino, J.; Giménez-Morera, A.; Novara, A.; Pulido, M.; Kapović-Solomun, M.; Keesstra, S.D. Policies can help to apply successful strategies to control soil and water losses: The case of chipped pruned branches (CPB) in Mediterranean citrus plantations. *Land Use Policy* **2018**, *75*, 734–745. [[CrossRef](#)]
13. Zhao, J.; Van Oost, K.; Chen, L.; Govers, G. Moderate topsoil erosion rates constrain the magnitude of the erosion-induced carbon sink and agricultural productivity losses on the Chinese Loess Plateau. *Biogeosciences* **2016**, *13*, 4735–4750. [[CrossRef](#)]
14. Rodrigo-Comino, J.; Iserloh, T.; Lassu, T.; Cerdà, A.; Keesstra, S.D.; Prosdocimi, M.; Brings, C.; Marzen, M.; Ramos, M.C.; Senciales, J.M.; et al. Quantitative comparison of initial soil erosion processes and runoff generation in Spanish and German vineyards. *Sci. Total Environ.* **2016**, *565*, 1165–1174. [[CrossRef](#)] [[PubMed](#)]
15. Thomas, J.; Joseph, S.; Thrivikramji, K.P. Assessment of soil erosion in a tropical mountain river basin of the southern Western Ghats, India using RUSLE and GIS. *Geosci. Front.* **2018**, *9*, 893–906. [[CrossRef](#)]
16. Keesstra, S.D.; Bouma, J.; Wallinga, J.; Tiftonell, P.; Smith, P.; Cerdà, A.; Montanarella, L.; Quinton, J.N.; Pachepsky, Y.; Van Der Putten, W.H.; et al. The significance of soils and soil science towards realization of the United Nations sustainable development goals. *Soil* **2016**, *2*, 111–128. [[CrossRef](#)]
17. Keesstra, S.; Mol, G.; de Leeuw, J.; Okx, J.; Molenaar, C.; de Cleen, M.; Visser, S. Soil-related sustainable development goals: Four concepts to make land degradation neutrality and restoration work. *Land* **2018**, *7*, 133. [[CrossRef](#)]
18. Wang, X.; Hu, S.; Wen, Q.; Yi, L.; Zuo, L.; Xu, J.; Zhang, Z.; Liu, B.; Zhao, X.; Liu, F. Assessment of soil erosion change and its relationships with land use/cover change in China from the end of the 1980s to 2010. *Catena* **2016**, *137*, 256–268. [[CrossRef](#)]
19. Bhattarai, R.; Dutta, D. Estimation of soil erosion and sediment yield using GIS at catchment scale. *Water Resour. Manag.* **2007**, *21*, 1635–1647. [[CrossRef](#)]
20. Kinnell, P.I.A. Event soil loss, runoff and the Universal Soil Loss Equation family of models: A review. *J. Hydrol.* **2010**, *385*, 384–397. [[CrossRef](#)]
21. Fu, B.J.; Zhao, W.W.; Chen, L.D.; Zhang, Q.J.; Lu, Y.H.; Gulinck, H.; Poesen, J. Assessment of soil erosion using RUSLE and GIS: A case study of the Yangou watershed in the Loess Plateau, China. *Land Degrad. Dev.* **2005**, *16*, 73–85. [[CrossRef](#)]
22. Cohen, M.J.; Shepherd, K.D.; Walsh, M.G. Empirical reformulation of the universal soil loss equation for erosion risk assessment in a tropical watershed. *Geoderma* **2005**, *124*, 235–252. [[CrossRef](#)]
23. Napoli, M.; Cecchi, S.; Orlandini, S.; Mugnai, G.; Zanchi, C.A. Simulation of field-measured soil loss in Mediterranean hilly areas (Chianti, Italy) with RUSLE. *Catena* **2016**, *145*, 246–256. [[CrossRef](#)]
24. Yang, X.; Gray, J.; Chapman, G.; Zhu, Q.; Tulau, M.; McInnes-Clarke, S. Digital mapping of soil erodibility for water erosion in New South Wales, Australia. *Soil Res.* **2017**, *56*, 158–170. [[CrossRef](#)]
25. Kijowska-Strugała, M.; Bucala-Hrabia, A.; Demczuk, P. Long-term impact of land use changes on soil erosion in an agricultural catchment (in the Western Polish Carpathians). *Land Degrad. Dev.* **2018**, *29*, 1871–1884. [[CrossRef](#)]
26. Kumar, S.; Kushwaha, S.P.S. Modelling soil erosion risk based on RUSLE-3D using GIS in a Shivalik sub-watershed. *J. Earth Syst. Sci.* **2013**, *122*, 389–398. [[CrossRef](#)]
27. Farhan, Y.; Nawaiseh, S. Spatial assessment of soil erosion risk using RUSLE and GIS techniques. *Environ. Earth Sci.* **2015**, *74*, 4649–4669. [[CrossRef](#)]
28. Zhang, P.; Yao, W.; Liu, G.; Xiao, P. Experimental study on soil erosion prediction model of loess slope based on rill morphology. *Catena* **2019**, *173*, 424–432. [[CrossRef](#)]
29. Smith, D.D.; Wischmeier, W.H. Factors affecting sheet and rill erosion. *Trans. Am. Geophys. Union* **1957**, *38*, 889–896. [[CrossRef](#)]

30. Wischmeier, W.H.; Smith, D.D. *Predicting Rainfall Erosion Losses: A Guide to Conservation Planning*; Agriculture Handbook No. 537; US Department of Agriculture Science and Education Administration: Washington, DC, USA, 1978; p. 163.
31. McCool, D.K.; Brown, L.C.; Foster, G.R.; Mutchler, C.K. Revised slope steepness factor for the Universal Soil Loss Equation. *Trans. ASAE* **1987**, *30*, 1387–1396. [[CrossRef](#)]
32. Liu, B.Y.; Nearing, M.A.; Shi, P.J.; Jia, Z.W. Slope length effects on soil loss for steep slopes. *Soil Sci. Soc. Am. J.* **2000**, *64*, 1759–1763. [[CrossRef](#)]
33. Liu, B.; Song, C.; Shi, Z.; Tao, H. Correction algorithm of slope factor in Universal Soil Loss Equation in earth-rocky mountain area of Southwest China. *Soil Water Conserv. China* **2015**, *8*, 49–52. (In Chinese)
34. Williams, J.R.; Jones, C.A.; Dyke, P.T. A modeling approach to determining the relationship between erosion and soil productivity. *Trans. ASAE* **1984**, *27*, 129–144. [[CrossRef](#)]
35. Zhang, K.L.; Shu, A.P.; Xu, X.L.; Yang, Q.K.; Yu, B. Soil erodibility and its estimation for agricultural soils in China. *J. Arid Environ.* **2008**, *72*, 1002–1011. [[CrossRef](#)]
36. Poesen, J.; De Luna, E.; Franca, A.; Nachtergaele, J.; Govers, G. Concentrated flow erosion rates as affected by rock fragment cover and initial soil moisture content. *Catena* **1999**, *36*, 315–329. [[CrossRef](#)]
37. Rodrigo-Comino, J.; García-Díaz, A.; Brevik, E.C.; Keesstra, S.D.; Pereira, P.; Novara, A.; Jordán, A.; Cerdà, A. Role of rock fragment cover on runoff generation and sediment yield in tilled vineyards. *Eur. J. Soil Sci.* **2017**, *68*, 864–872. [[CrossRef](#)]
38. Cerdà, A. Effects of rock fragment cover on soil infiltration, interrill runoff and erosion. *Eur. J. Soil Sci.* **2001**, *52*, 59–68. [[CrossRef](#)]
39. Poesen, J.W.; Torri, D.; Bunte, K. Effects of rock fragments on soil erosion by water at different spatial scales: A review. *Catena* **1994**, *23*, 141–166. [[CrossRef](#)]
40. Jomaa, S.; Barry, D.A.; Heng, B.C.P.; Brovelli, A.; Sander, G.C.; Parlange, J.Y. Influence of rock fragment coverage on soil erosion and hydrological response: Laboratory flume experiments and modeling. *Water Resour. Res.* **2012**, *48*, W05535. [[CrossRef](#)]
41. Shi, C. Effects of gravel content on soil erodibility and the methods of estimating soil erodibility factor K. *Chin. J. Soil Sci.* **2009**, *40*, 1398–1401. (In Chinese)
42. Sun, W.Y.; Shao, Q.Q.; Liu, J.Y.; Zhai, J. Assessing the effects of land use and topography on soil erosion on the Loess Plateau in China. *Catena* **2014**, *121*, 151–163. [[CrossRef](#)]
43. Zhang, Z.; Gao, J.; Gao, Y. The influences of land use changes on the value of ecosystem services in Chaohu Lake Basin, China. *Environ. Earth Sci.* **2015**, *74*, 385–395. [[CrossRef](#)]
44. Renard, K.G.; Foster, G.R.; Weesies, G.A. *Predicting Soil Erosion by Water: A Guide to Conservation Planning with the Revised Universal Soil Loss Equation (RUSLE)*; Agriculture Handbook No. 703; US Department of Agriculture Science and Education Administration: Washington, DC, USA, 1997; pp. 1–251.
45. Antoneli, V.; Rebinski, E.; Bednarz, J.; Rodrigo-Comino, J.; Keesstra, S.; Cerdà, A.; Pulido Fernández, M. Soil Erosion Induced by the Introduction of New Pasture Species in a Faxinal Farm of Southern Brazil. *Geosciences* **2018**, *8*, 166. [[CrossRef](#)]
46. Rodrigo-Comino, J.; Keesstra, S.D.; Cerdà, A. Connectivity assessment in Mediterranean vineyards using improved stock unearthing method, LiDAR and soil erosion field surveys. *Earth Surf. Process. Landf.* **2018**, *43*, 2193–2206. [[CrossRef](#)]
47. Mondal, A.; Khare, D.; Kundu, S. International Soil and Water Conservation Research Change in rainfall erosivity in the past and future due to climate change in the central part of India. *Int. Soil Water Conserv. Res.* **2016**, *4*, 186–194. [[CrossRef](#)]
48. Amanambu, A.C.; Li, L.; Egbinola, C.N.; Obarein, O.A.; Mupenzi, C.; Chen, D. Spatio-temporal variation in rainfall-runoff erosivity due to climate change in the Lower Niger Basin, West Africa. *Catena* **2019**, *172*, 324–334. [[CrossRef](#)]
49. Teng, H.; Shi, Z.; Ma, Z.; Li, Y. Estimating spatially downscaled rainfall by regression kriging using TRMM precipitation and elevation in Zhejiang Province, southeast China. *Int. J. Remote Sens.* **2014**, *35*, 7775–7794. [[CrossRef](#)]
50. Liu, B.; Tao, H.; Song, C.; Guo, B.; Shi, Z.; Zhang, C.; Kong, B.; He, B. Temporal and spatial variations of rainfall erosivity in China during 1960 to 2009. *Geogr. Res.* **2013**, *32*, 245–256. (In Chinese)
51. Karydas, C.; Petriolis, M.; Manakos, I. Evaluating alternative methods of soil erodibility mapping in the mediterranean island of Crete. *Agriculture* **2013**, *3*, 362–380. [[CrossRef](#)]

52. Lin, B.S.; Chen, C.K.; Thomas, K.; Hsu, C.K.; Ho, H.C. Improvement of the K-Factor of USLE and soil erosion estimation in Shihmen reservoir watershed. *Sustainability* **2019**, *11*, 355. [[CrossRef](#)]
53. Wang, M.; Baartman, J.E.M.; Zhang, H.; Yang, Q.; Li, S.; Yang, J.; Cai, C.; Wang, M.; Ritsema, C.J.; Geissen, V. An integrated method for calculating DEM-based RUSLE LS. *Earth Sci. Inform.* **2018**, *11*, 579–590. [[CrossRef](#)]
54. Yang, X. Digital mapping of RUSLE slope length and steepness factor across New South Wales, Australia. *Soil Res.* **2015**, *53*, 216–225. [[CrossRef](#)]
55. Xue, J.; Lyu, D.; Wang, D.; Wang, Y.; Yin, D.; Zhao, Z.; Mu, Z. Assessment of soil erosion dynamics using the GIS-Based RUSLE Model: A case study of wangjiagou watershed from the Three Gorges Reservoir Region, Southwestern China. *Water* **2018**, *10*, 1817. [[CrossRef](#)]
56. Zha, L.; Deng, G.; Gu, J. Dynamic changes of soil erosion in the Chaohu Watershed from 1992 to 2013. *Acta Geogr. Sin.* **2015**, *70*, 1708–1719. (In Chinese)
57. Li, L.; Canters, F.; Solana, C.; Ma, W.; Chen, L.; Kervyn, M. Discriminating lava flows of different age within Nyamuragira’s volcanic field using spectral mixture analysis. *Int. J. Appl. Earth Obs. Geoinf.* **2015**, *40*, 1–10. [[CrossRef](#)]
58. Li, H.; Li, L.; Chen, L.; Zhou, X.; Cui, Y.; Liu, Y.; Liu, W. Mapping and Characterizing Spatiotemporal Dynamics of Impervious Surfaces Using Landsat Images: A Case Study of Xuzhou, East China from 1995 to 2018. *Sustainability* **2019**, *11*, 1224. [[CrossRef](#)]
59. Zhou, X.; Li, L.; Chen, L.; Liu, Y.; Cui, Y. Discriminating Urban Forest Types from Sentinel-2A Image Data through Linear Spectral Mixture Analysis: A Case Study of Xuzhou, East China. *Forests* **2019**, *10*, 478. [[CrossRef](#)]
60. Lu, D.; Li, G.; Valladares, G.S.; Batistella, A.M. Mapping soil erosion risk in Rondônia, Brazilian Amazonia: Using RUSLE, remote sensing and GIS. *Land Degrad. Dev.* **2004**, *15*, 499–512. [[CrossRef](#)]
61. Markose, V.J.; Jayappa, K.S. Soil loss estimation and prioritization of sub-watersheds of Kali River basin, Karnataka, India, using RUSLE and GIS. *Environ. Monit. Assess.* **2016**, *188*, 225–240. [[CrossRef](#)]
62. Li, L.; Bakelants, L.; Solana, C.; Canters, F.; Kervyn, M. Dating lava flows of tropical volcanoes by means of spatial modeling of vegetation recovery. *Earth Surf. Process. Landf.* **2017**, *43*, 840–856. [[CrossRef](#)]
63. Amri, R.; Zribi, M.; Lili-Chabaane, Z.; Duchemin, B.; Gruhier, C.; Chehbouni, A. Analysis of vegetation behavior in a North African semi-arid region, Using SPOT-VEGETATION NDVI data. *Remote Sens.* **2011**, *3*, 2568–2590. [[CrossRef](#)]
64. Gutman, G.; Ignatov, A. The derivation of the green vegetation fraction from NOAA/AVHRR data for use in numerical weather prediction models. *Int. J. Remote Sens.* **1998**, *19*, 1533–1543. [[CrossRef](#)]
65. Van der Knijff, J.M.; Jones, R.J.A.; Montanarella, L. *Soil Erosion Risk Assessment in Europe*; European Soil Bureau, Joint Research Centre, European Commission and Space Applications Institute: Brussel, Belgium, 2000; pp. 17–19.
66. Panagos, P.; Borrelli, P.; Meusburger, K.; van der Zanden, E.H.; Poesen, J.; Alewell, C. Modelling the effect of support practices (P-factor) on the reduction of soil erosion by water at European scale. *Environ. Sci. Policy* **2015**, *51*, 23–34. [[CrossRef](#)]
67. Borrelli, P.; Alewell, C.; Ballabio, C.; Ferro, V.; Robinson, D.A.; Panagos, P.; Lugato, E.; Van Oost, K.; Schütt, B.; Fleischer, L.R.; et al. An assessment of the global impact of 21st century land use change on soil erosion. *Nat. Commun.* **2013**, *8*, 1–13. [[CrossRef](#)] [[PubMed](#)]
68. Cui, Y.; Li, L.; Chen, L.; Zhang, Y.; Cheng, L.; Zhou, X.; Yang, X. Land-use carbon emissions estimation for the Yangtze River Delta Urban Agglomeration using 1994–2016 Landsat image data. *Remote Sens.* **2018**, *10*, 1334. [[CrossRef](#)]
69. Ministry of Water Resources of the People’s Republic of China. *Standards for Classification and Gradation of Soil Erosion (SL190-2007)*; China Water&Power Press: Beijing, China, 2007.
70. Hewett, C.J.M.; Simpson, C.; Wainwright, J.; Hudson, S. Communicating risks to infrastructure due to soil erosion: A bottom-up approach. *Land Degrad. Dev.* **2018**, *29*, 1282–1294. [[CrossRef](#)]
71. Liu, Y.; Shi, Z.; Chappell, A.; Liang, Z.; Chen, S.; Yu, W.; Teng, H.; Viscarra Rossel, R.A. Current and future assessments of soil erosion by water on the Tibetan Plateau based on RUSLE and CMIP5 climate models. *Sci. Total Environ.* **2018**, *635*, 673–686.
72. Moges, D.M.; Bhat, H.G. Integration of geospatial technologies with RUSLE for analysis of land use/cover change impact on soil erosion: Case study in Rib watershed, north-western highland Ethiopia. *Environ. Earth Sci.* **2017**, *76*, 1–14. [[CrossRef](#)]

73. Bryan, R.B. Soil erodibility and processes of water erosion on hillslope. *Geomorphology* **2000**, *32*, 385–415. [[CrossRef](#)]
74. Wang, L.; Huang, J.; Du, Y.; Hu, Y.; Han, P. Dynamic assessment of soil erosion risk using landsat TM and HJ satellite data in danjiangkou reservoir area, China. *Remote Sens.* **2013**, *5*, 3826–3848. [[CrossRef](#)]
75. Mandal, D.; Sharda, V.N. Appraisal of soil erosion risk in the Eastern Himalayan Region of India for soil conservation planning. *Land Degrad. Dev.* **2013**, *24*, 430–437. [[CrossRef](#)]
76. Wynants, M.; Solomon, H.; Ndakidemi, P.; Blake, W.H. Pinpointing areas of increased soil erosion risk following land cover change in the Lake Manyara catchment, Tanzania. *Int. J. Appl. Earth Obs. Geoinf.* **2018**, *71*, 1–8. [[CrossRef](#)]
77. Alexakis, D.D.; Hadjimitsis, D.G.; Agapiou, A. Integrated use of remote sensing, GIS and precipitation data for the assessment of soil erosion rate in the catchment area of “Yialias” in Cyprus. *Atmos. Res.* **2013**, *131*, 108–124. [[CrossRef](#)]
78. Yang, Z.S. The Topographic factor of soil erosion of sloping cultivated land in the northeast mountain region of Yunnan Province. *J. Mt. Sci.* **1999**, *17*, 16–18.
79. Mu, E.S. Analysis on runoff yield characteristics of slope surface runoff under different control measure conditions in Shiqiao small watershed of Karst Area. *J. Anhui Agric. Sci.* **2012**, *40*, 939–941.
80. Bi, X.G.; Duan, S.H.; Li, Y.G.; Liu, B.Y.; Fu, S.H.; Ye, Z.H.; Yuan, A.P.; Lu, B.J. Study on soil loss equation in Beijing. *Sci. Soil Water Conserv.* **2006**, *4*, 6–13.
81. Tang, K.L.; Xiong, G.S.; Liang, J.Y.; Jing, K.; Zhang, S.L.; Chen, Y.Z.; Li, S.M. *Varieties of erosion and runoff sediment in Yellow River*; Chinese Sciences and Technique Press: Beijing, China, 1993; pp. 155–162.
82. Zhang, L. Study on the Influence of Slope Factor of Longitudinal Ridge Valley on Soil Erosion. Master’s Thesis, Kunming University of Science and Technology, Kunming, China, 2008.
83. Xu, J.; Wang, Y.; Sun, J.H.; Chen, Z.J.; Xue, C.K.; Xu, Z.H.; Wang, X.R. Effects of slope factor on soil erosion in Jinan city. *J. Univ. Jinan* **2017**, *31*, 433–437.
84. Wang, X.Y.; Cao, W.H.; Chen, D. Study on relationship between soil erosion and land slope. *J. Sediment Res.* **1998**, *2*, 36–41.
85. Lin, J.L.; Cai, Z.F.; Chen, M.H.; Zhou, F.J.; Huang, Y.H. Relationship between slope degree and soil erosion in the south Fujian. *Fujian J. Agric. Sci.* **2002**, *17*, 86–89.
86. Wu, N.N.; Liang, Y.H.; Zhang, J.M.; Ma, L.S. Soil erosion characteristics of different slope gradients and aspects: Taking low mountain and hilly areas in north branches of Huaihe River as an Example. *Hubei Agric. Sci.* **2014**, *53*, 3755–3759.
87. Liu, S.Y.; Qin, F.C.; Xiang, Y.H.; Lei, F.Y. Study on the relationship between slope and the amount of soil loss based on WEPP. *J. Arid Land Resour. Environ.* **2006**, *20*, 97–101.

